JOURNAL OF CATALYSIS 144, 175–192 (1993)

Low-Temperature Oxidation of CO over Gold Supported on TiO_2, α-Fe_2O_3, and Co_3O_4

MASATAKE HARUTA,*,[1] SUSUMU TSUBOTA,* TETSUHIKO KOBAYASHI,*
HIROYUKI KAGEYAMA,* MICHEL J. GENET,†
AND BERNARD DELMON†

*Government Industrial Research Institute of Osaka, Midorigaoka 1, Ikeda, 563 Japan; and †Université Catholique de Louvain, Groupe Physico-Chimie Minérale et de Catalyse, Place Croix du Sud 1, B1348 Louvain-la-Neuve, Belgium

Received January 6, 1993; revised June 14, 1993

Gold can be highly dispersed on a variety of metal oxides by coprecipitation and deposition–precipitation followed by calcination in air. The small gold particles are hemispherical in shape and stabilized by epitaxial contact, dislocations, or contact with an amorphous oxide layer. Such supported gold differs in catalytic nature from unsupported gold particles and exhibits high catalytic activities for low-temperature oxidation of CO. Especially, gold supported on TiO_2, α-Fe_2O_3, Co_3O_4, NiO, $Be(OH)_2$, and $Mg(OH)_2$ is very active even at temperatures below 0°C. Among the gold catalysts supported on TiO_2, α-Fe_2O_3, and Co_3O_4 the turnover frequencies for CO oxidation per surface gold atom are almost independent of the kind of support oxides used and increase sharply with a decrease in diameter of gold particles below 4 nm. Small gold particles not only provide the sites for the reversible adsorption of CO but also appreciably increase the amount of oxygen adsorbed on the support oxides. In the temperature range −10 to 65°C, the activation energies for CO oxidation were 8.2 kcal/mol (Au/TiO_2), 8.4 kcal/mol (Au/α-Fe_2O_3), and 3.9 kcal/mol (Au/Co_3O_4). The rate of CO oxidation is zero order with respect to CO for the three catalysts, and 0.2–0.3 for Au/TiO_2 and Au/Co_3O_4 and zero order for Au/α-Fe_2O_3 with respect to O_2. By taking into consideration TPD and FT-IR data, a mechanism is proposed in which CO adsorbed on gold particles migrates toward the perimeter on support oxides and there it reacts with adsorbed oxygen to form bidentate carbonate species. The decomposition of the carbonate intermediate is considered to be rate-determining.

INTRODUCTION

Gold has long been regarded as catalytically far less active than platinum group metals (*1, 2*). However, our work (*3–8*) and recent publications by other groups (*9–14*) have clearly shown that gold is remarkably active for low-temperature oxidation of CO when it is highly dispersed and deposited on reducible semiconductor metal oxides, hydroxides of alkaline earth metals, or amorphous ZrO_2. In addition, our recent work has also revealed that by selecting suitable metal oxides as supports, gold becomes active for the catalytic combustion of hydrocarbons (*15, 16*), reduction of NO with CO to N_2 (*15, 17*), oxidative-decomposition of trimethylamine (*18*), and hydrogenation of CO and CO_2 (*15, 19*). In the hydrogenation of carbon oxides, gold has been selected to examine the Schottky barrier effect in the metal–metal oxide interface (*20–22*) and to compare catalytic activities among Group IB metals (*23*).

Since it has been shown that the activities of the above supported gold catalysts for low-temperature CO oxidation are enhanced by moisture, some of them are already commercialized to remove odor and CO in air at room temperature (*24*). Commercial applications have also been extended to selective CO gas sensors (*25, 26*), and our commercial gold catalysts and a Au/Fe_2O_3 catalyst prepared by another group

[1] To whom correspondence should be addressed.

0021-9517/93 $5.00

have been tested for sealed CO_2 lasers (*27, 28*). These successes are understood to be mainly due to the careful preparation of supported gold for achieving high dispersion on a variety of metal oxide supports, because as far as the conventional impregnation method is used, the supported gold catalysts obtained exhibit no appreciable activity.

As pointed out by Zhang (*29*), it is very difficult to obtain gold in a state of dispersion as high as those of platinum and palladium. This is mainly because the melting point of gold at 1063°C is much lower than those of Pt (1769°C) and Pd (1550°C). It has been reported that the melting point of gold particles with a diameter of 2 nm is lowered to 300°C due to the quantum size effect (*30*). Accordingly, we should pay much attention to the dispersion of gold when we attempt to discuss catalysis by gold and gold-reducible metal oxide interfaces in comparison with the systems composed of the other Group IB metals or Pt-group metals. This point of view is lacking in most of the earlier work on supported gold catalysts, and discrepancies in the reported experimental results have caused confusion and controversy. On the other hand, since gold itself is known to be very inactive, any enhanced activity in Au–metal oxide systems could be solely attributed to the electronic interaction and/or the active sites on the interfacial perimeter resulting from the gold deposition on a support.

In view of the growing interest in gold as an outstanding example for a study of metal–support interaction, the present paper deals with the interrelation between preparation, fine structure, and catalytic properties of gold deposited on a variety of metal oxides, most specifically TiO_2, α-Fe_2O_3, and Co_3O_4. Based on spectroscopic and kinetic investigations, a mechanism is also proposed that can explain the auspicious increase of activity in the oxidation of CO at low temperatures observed with supported gold.

EXPERIMENTAL

Preparation of Catalysts

In a series of experiments performed to investigate the effect of metal oxide support on the catalytic activities for the oxidation of H_2 and CO, all the samples had a metal loading expressed as atomic ratio of Au/Me = 1/19 (where Me is the metal of oxide support) and except for Au/SiO_2 were prepared by coprecipitation. An aqueous mixture of $HAuCl_4$ and a nitrate of the corresponding metal oxide support was poured into an aqueous solution of Na_2CO_3. The coprecipitate was washed and then dried under vacuum overnight and finally calcined in air at 400°C for 5 h, except when otherwise denoted. Gold on SiO_2 was prepared by deposition–precipitation in a $HAuCl_4$ solution containing gold at an atomic ratio of 1/19 with respect to Si followed by calcination at 300°C. Deposition–precipitation followed by calcination at 400°C was also used in depositing Au on TiO_2 and Al_2O_3 in order to compare the catalytic activity with that of catalysts obtained by coprecipitation. After washing and drying, the precursor was calcined at 400°C for 4 h. The gold content in the catalyst obtained was about 3.3 wt%.

For mechanistic investigations on the size effect of gold particles, kinetic behavior, TPD, and FT-IR, three types of catalysts, namely, Au/Co_3O_4, Au/α-Fe_2O_3, and Au/TiO_2 (anatase), were prepared by deposition–precipitation followed by washing, drying, and calcination in air at 400°C for 4 h. The supports of Co_3O_4 and α-Fe_2O_3 were prepared by calcining the precipitates in air at 400°C, with the precipitates obtained by neutralizing the nitrates of the corresponding metal oxides by Na_2CO_3. The specific surface areas were 59 m^2/g for Co_3O_4 and 37 m^2/g for α-Fe_2O_3. The titanium dioxide used was JRC-TIO-4, a reference catalyst provided by the Catalysis Society of Japan, with a specific surface area of 50 m^2/g. The detailed preparation conditions for Au/TiO_2 have been described elsewhere (*8*). The reason why we have chosen deposition–precipitation for the studies mentioned above is

because not only can it produce metallic gold particles with a narrow size distribution but also it prevents the copresence of the rafts of gold clusters, which were often observed in coprecipitated samples. The gold contents, which were determined for the calcined samples by X-ray fluorescence spectroscopy (Rigaku, System 3370), were varied in the range 0.5 to 8 wt% on an Au/metal oxide basis. The particle size of gold was controlled by changing pH and the concentration of $HAuCl_4$ in the starting solutions.

In order to clearify the significant role of gold, a blank sample was prepared for α-Fe_2O_3 by precipitation from an aqueous solution of $Fe(NO_3)_3$ containing Cl^- at a concentration that would have attended the presence of $HAuCl_4$. Elemental analyses of Pd, Pt, and Ir impurities were conducted by means of atomic emission spectroscopy using an inductively coupled argon plasma source (Hitachi Ltd., ICP Emission Analysis System 306) for the $HAuCl_4 \cdot 4H_2O$, the Au/TiO_2 prepared by deposition–precipitation, and the Au/α-Fe_2O_3 prepared by coprecipitation.

Activity Measurements

Standard catalytic activity measurements were carried out in a fixed bed reactor using 200 mg of catalysts of 70 to 120 mesh size. A standard gas containing 1 vol% H_2 or CO in air was dried in a silica gel and P_2O_5 column and passed through the catalyst bed at a rate of 67 ml/min (SV = 20,000 $h^{-1} \cdot$ ml/g-cat.). For measurements performed at temperatures below 0°C, the reaction gases were additionally dried by a silica gel column maintained at −77°C. For kinetic studies, the reaction gas (with different concentrations of CO and O_2 in N_2 depending on experiment) was dehydrated in a molecular sieve column and passed through the catalyst bed containing 50-mg catalyst samples diluted with 500 mg of quartz powder. The conversions of H_2 and CO were determined by analyzing effluent gases with a gas chromatography. In kinetic experiments, the conversions of CO were principally kept below 10% to analyze the data based on a differential reactor model.

Characterization

The particle size of gold was determined by a high-resolution TEM (Hitachi H-9000). At least 200 particles were chosen to determine the mean diameter by using a computerized image analyzer (EXCEL, Nippon Avionics Co. Ltd.). EXAFS (extended X-ray absorption fine structure) measurements were performed at Beam Line 10B of the 2.5-GeV storage ring of Photon Factory in the National Laboratory for High Energy Physics (KEK, Tsukuba). For the Au–Fe coprecipitated precursor dried or calcined at different temperatures, X-ray absorption data was collected at 60 K and for Au_2O_3 and Au foil references at 300 K. Data analysis was made according to the procedure described before (*31*). XPS measurements were conducted in Université Catholique de Louvain (Belgium) by using an SSX/206 spectrometer (FISONS-Surface Science Instruments) with a monochromatized Al focused X-ray beam and an analyzer energy of 50 eV. The FWHM (full width at half maximum) of the $Au_{4f7/2}$ peak of bulk metallic gold was around 1.0 eV. The binding energies were calculated by reference to the binding energy of the C–(C, H) component of the C1*s* contamination peak assumed at 285.0 eV. TPD measurements were carried out by using an apparatus equipped with a TCD detector after treating the samples in an O_2 or He stream at 400°C for 10 h and then cooling to 0°C. After CO injection, the desorbed species were identified by a quadrupole mass analyzer (ANELVA AQA-100 MPX). FT-IR measurements were conducted at room temperature by using Nicolet 20SXC after pretreating the samples in an He stream at 200°C for 30 min.

RESULTS

Impurities Measurements

The impurity levels of Pd, Pt, and Ir in the $HAuCl_4 \cdot 4H_2O$ reagent used were ap-

proximately 11, 2, and 7 ppm, respectively. In the Au/TiO_2 catalyst prepared by deposition–precipitation in an aqueous $HAuCl_4$ solution, with Au at a metal loading of 13.0 wt%, the Au content was 2.3 wt% and the contamination by Pd, Pt, and Ir was below the detection level; Pd < 50 ppm, Pt < 5 ppm, and Ir < 50 ppm. In the case of Au/α-Fe_2O_3 prepared by coprecipitation in an aqueous $HAuCl_4$ containing Au at a metal loading of 13.0 wt%, the Au content was 11.3 wt% and the contamination by Pd, Pt, and Ir was below the detection level: Pd < 3 ppm, Pt < 3 ppm, Ir < 30 ppm. Detection levels of Ir in both Au/TiO_2 and Au/α-Fe_2O_3 and that of Pd in Au/TiO_2 were relatively high because of the influence of coexisting metal cations present in the support oxides.

Since the precursors obtained by deposition–precipitation or coprecipitation were thoroughly washed with distilled water before drying and calcining, the concentration of remaining impurities can be considered to be close to negligible. On the other hand, the conventional impregnation method does not include a washing process, so leaving all the impurities behind in the catalyst. Accordingly, the catalytic activities observed in the present study, which are markedly high in comparison with those of impregnated gold catalysts and Pt group metal catalysts, can not be ascribed to the contamination by Pd, Pt, and Ir. It should also be noted that for the oxidation of CO these noble metals of Group VIII are not active at temperatures below 150°C (*32*).

Structures of Supported Gold Catalysts Prepared by Coprecipitation

The Fourier transforms of EXAFS in Fig. 1 typically show how gold species in the Au–Fe coprecipitated precursors change after drying and calcining in air at different temperatures. At 200°C and below this temperature, gold can exist as an oxidic species similar to hydrous gold oxide, Au_2O_3. Because simple gold oxide is readily decomposed to metallic gold even at 80°C, this result shows that oxidic gold is thermally

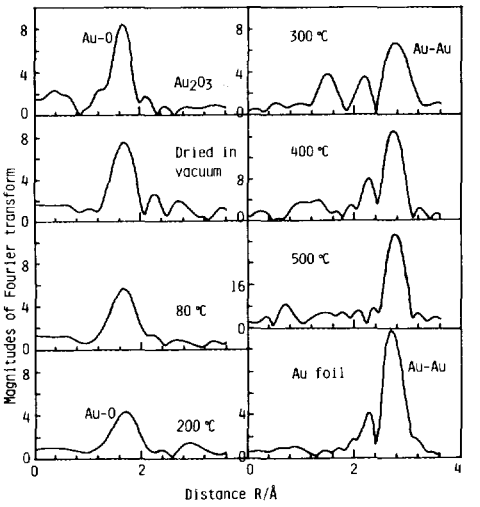

FIG. 1. Fourier transforms of k^3-weighted EXAFS oscillation about Au L_3-edge measured at 60 K for Au–Fe(1 : 19) coprecipitate calcined at various temperatures.

stabilized on mixing with ferric hydroxide. At 300°C the oxidic gold species are mostly decomposed into metallic species. However, at this temperature the coexistence of oxidic species was also seen in the so-called white line of the Au L_3 X-ray absorption near edge spectrum (XANES) as a sharp peak. The peak area ratio of the oxidic gold species in the 300°C sample to neat Au_2O_3 measured at 300 K was calculated to be about 0.2. At 400°C almost all oxidic gold species are decomposed into metallic species, which was also evidenced by the absence of a significant peak in the white line area. The change in gold species from oxidic to metallic is accompanied by the transformation of amorphous ferric hydroxide into crystalline hematite (α-Fe_2O_3), as proven by powder X-ray diffraction measurements and Mössbauer spectroscopy (*33*).

Figure 2a shows a TEM photograph of the Au-Fe coprecipitate calcined at 400°C. As can be seen, small gold particles are homogeneously dispersed on α-Fe_2O_3 particles. The mean particle diameter of Au was 3.6 nm with a standard deviation of 1.3 nm. The coordination number of Au atom was

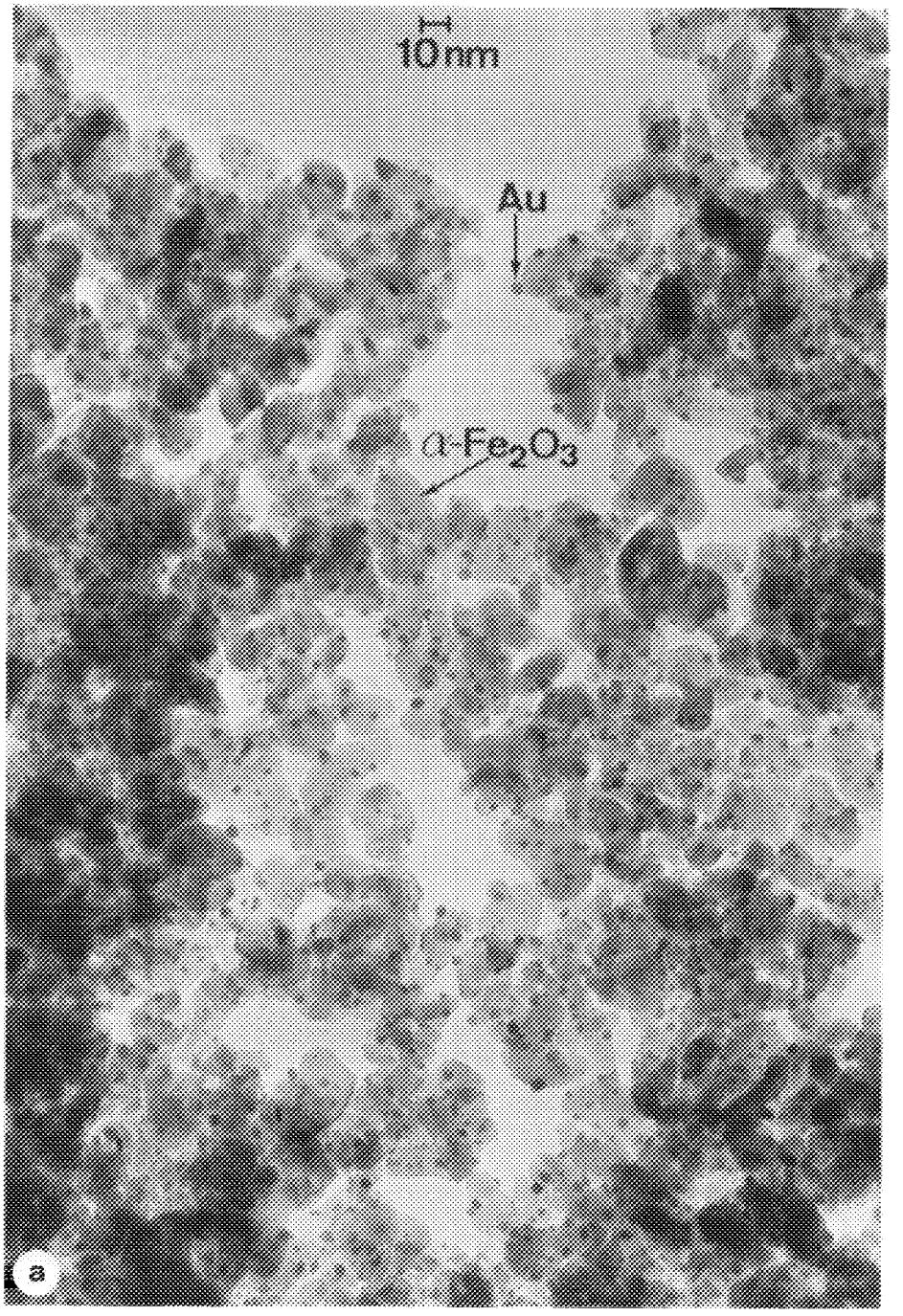

FIG. 2. TEM photographs of Au–Fe(1 : 19) coprecipitate calcined at 400°C: (a) dispersion of gold particles over α-Fe_2O_3 and (b) specific crystal orientation of gold particles with respect to α-Fe_2O_3.

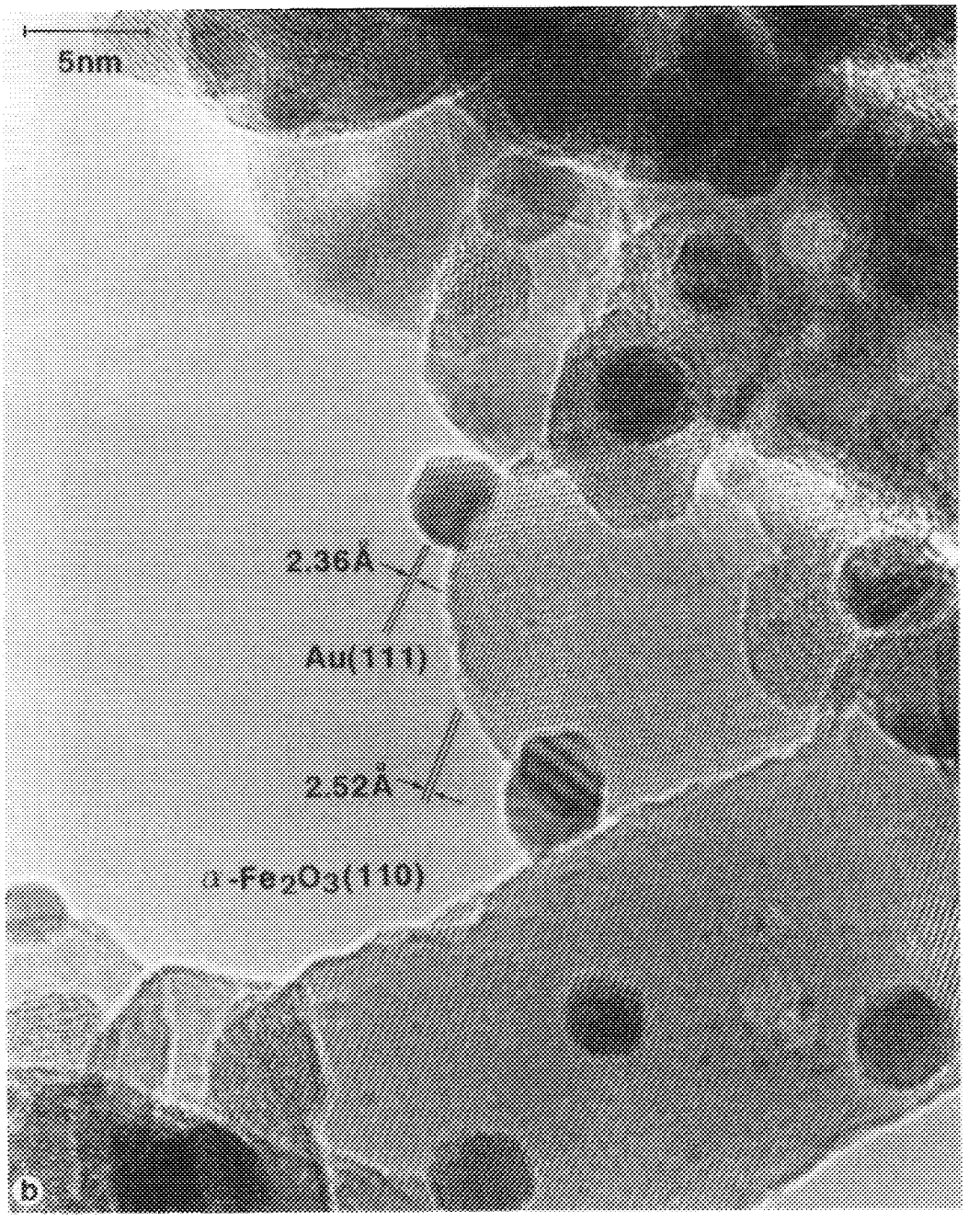

FIG. 2—*Continued*

evaluated from the EXAFS data to be 8–10, which corresponded to hemispherical Au particles with a diameter of 1.5–3 nm. Since X-ray diffraction pattern showed a small broad peak corresponding to Au(111), the diameter of Au was estimated by using Sher-

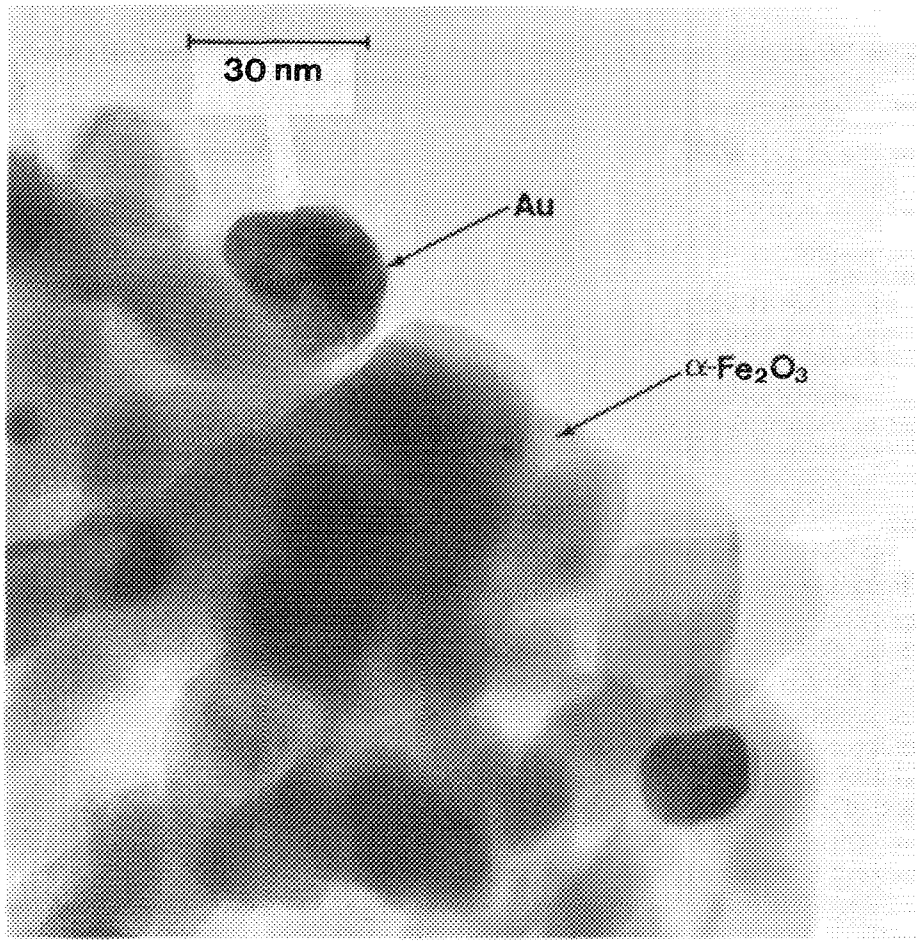

FIG. 3. TEM photograph of Au deposited on α-Fe_2O_3 by impregnation followed by reduction with H_2 at 90°C. Gold loading is 1.0 wt%.

rer's equation to be around 3.6 nm. In the sample prepared by the conventional impregnation method, as can be seen in Fig. 3, gold particles were very large, having diameters from 10 to 30 nm, although the metal loading was only 1 wt% and the dried impregnated precursor was reduced in an H_2 stream at a temperature as low as 90°C. This catalyst was the most active among the impregnated gold catalysts with different Au loadings which were washed with hot water to remove Cl^- and dried again, however, the oxidation of CO took place only at temperatures above 0°C. Therefore, it is clear that coprecipitation is much superior to impregnation for obtaining a high dispersion of gold and accordingly enhanced support effect.

A high magnification TEM photograph in Fig. 2b shows in the cross sectional view that gold particles are not spherical but hemispherical in shape and that they are attached to the support by their flat plane, with a specific crystal orientation with respect to the support. In coprecipitated samples containing 3*d* transition metals of Group VIII, a specific crystal orientation was often observed at the interface between

TABLE 1

Crystal Nature of the Interface between Gold and Metal Oxide in the Supported Gold Catalysts Prepared by Coprecipitation

Gold:			
Mean particle diameter (nm)	4.0	6 ~ 7	7 ~ 8
Crystal plane at the interface	111	111	111
(lattice distance Å)	(2.36)	(2.36)	(2.36)
Metal oxide support:			
Type of oxides	α-Fe_2O_3	Co_3O_4	NiO
Mean particle diameter (nm)	40	20	10
Crystal plane at the interface	110	111	111
(lattice distance Å)	(2.52)	(4.67)	(2.41)
Possibility of epitaxial contact indicated by computer graphics	No	Yes	Yes

gold and the support oxides, as shown in Table 1 (*6*). Gold is always deposited with its 111 plane in contact with the oxide. The spacings of the crystal planes of metal oxides are so close to the lattice spacing of gold (2.36 Å) or two times this value that epitaxial growth is very likely. To know whether the contacts are really epitaxial or not, it is also necessary in principle to take a top view of the atomic configuration at the interface. This was impossible because the samples were in powder form and the gold particles were too thick. We only investigated possible atomic configurations at the interface by computer graphics (*34*). The results are tabulated in the last row in Table 1. A careful observation of Fig. 2b also indicates that, in addition to gold particles with a size of 4 nm, there are also very tiny shadowed spots. Atomic-scale investigation by TEM has revealed that these are the rafts of gold clusters of about three atoms wide and one monolayer thick (*35*).

The interfaces between gold and metal oxide thus appear to be in tight contact exhibiting specific crystal orientation. The small hemispherical gold particles, having a size of 3–4 nm in diameter, are composed of less than 1000 atoms, about 40% of which are present at the surface and the gold/support interface. This strongly suggests that they might have an electronically different character compared to bulk gold.

Figure 4 shows XPS Au_{4f} spectra obtained for the Au–Fe coprecipitate calcined at 300°C and 400°C. The Au_{4f} peak for the 400°C sample, centered at 84.0 eV, shows an asymmetry toward higher binding energies, however, the position, amplitude, and FWHM were almost the same as those observed on the Au_{4f} peak of bulk metallic gold recorded in the same conditions. The $Au_{4f7/2}$ peak, therefore, corresponds probably to metallic gold, which can be correlated with small particles observed in TEM. For the 300°C sample, this asymmetry can not fully explain the peak broadening which was observed. Since the copresence of oxidic gold species was revealed in XANES, we made an attempt to decompose the peak by fixing a component at 84.0 eV and a second "nonmetallic" component could be assumed at a binding energy about 0.5 eV higher than that of the peak for bulk metallic gold. That shifted peak may be assigned to such small gold clusters as observed on the TEM micrograph in Fig. 2b, which are appreciably increased in fraction for the sample calcined at 300°C. Gold oxide (hydrous Au_2O_3) has a chemical shift of about 2.5 eV according to literature (*36*) and our own measurements, which implies that the gold clusters would lie electronically between metal Au^0 and cation, Au^+ or Au^{3+}. However, the samples having these gold clusters in addition to metallic gold particles were not catalytically

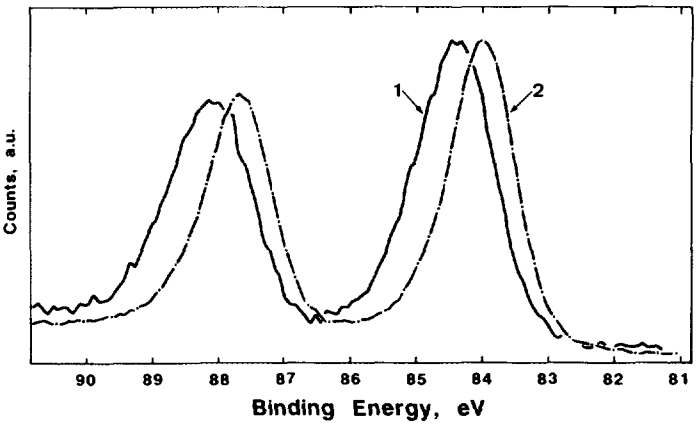

FIG. 4. XPS spectra of Au 4*f* electrons for Au–Fe(1 : 19) coprecipitate calcined at 300°C (curve 1) and at 400°C (curve 2).

more active than the samples without the gold clusters. From this result, metallic gold particles are regarded as being responsible for CO oxidation.

Structures of Supported Gold Catalysts Prepared by Deposition–Precipitation

In contrast to the well ordered crystalline interface observed for coprecipitated systems, deposition–precipitation usually gave rise to structures disordered with respect to the metal–oxide interface. In Fig. 5 dislocations are seen at a distance of around 2 nm inside from the outer surface of TiO_2. This may have resulted from the crystallization of the surface hydroxide layer formed during deposition-precipitation in aqueous solution. The crystalline surface is covered with an amorphous phase, in which small gold particles appear to be embedded. This interface structure might contribute to the stabilization of small gold particles against coalescence.

Catalytic Nature of Supported Gold

As a typical example, Fig. 6 compares the catalytic activities for the oxidation of H_2 and CO of unsupported gold particles with diameters around 20 nm, and gold supported on α-Fe_2O_3 and α-Fe_2O_3 alone. It should be noted that supported gold differs completely from unsupported gold in catalysis. Unsupported gold metal particles are poorly active for the oxidation of CO. However, they can catalyze the oxidation of H_2 at much lower temperatures. This feature is commonly observed with other noble metal catalysts like palladium supported on Al_2O_3. On the other hand, supported gold catalysts are extraordinarily active for CO oxidation. The reaction can take place even at -70°C, whereas hydrogen oxidation requires higher temperatures. This result appears to reflect the catalytic nature of α-Fe_2O_3, which is more active for CO oxidation than H_2 oxidation. The blank sample of α-Fe_2O_3 prepared by precipitation from an aqueous solution of $Fe(NO_3)_3$ in the copresence of Cl^- showed a much poorer activity (the temperature for 50% conversion of CO equals 280°C) than for samples prepared in the absence of Cl^-, thus proving that the remarkably high activities of the supported gold sample did not stem simply from the modification of the support or support-initiated radical reactions.

In the comparison between H_2 and CO oxidation, the effect of calcination temperature is also worth noting. Figure 7 shows that, in the case of the Au–Fe coprecipitate, the conversion of H_2 at 30°C is 40% for the sample dried at 80°C and reaches a maximum at temperatures between 200 and 300°C. On the other hand, for the samples

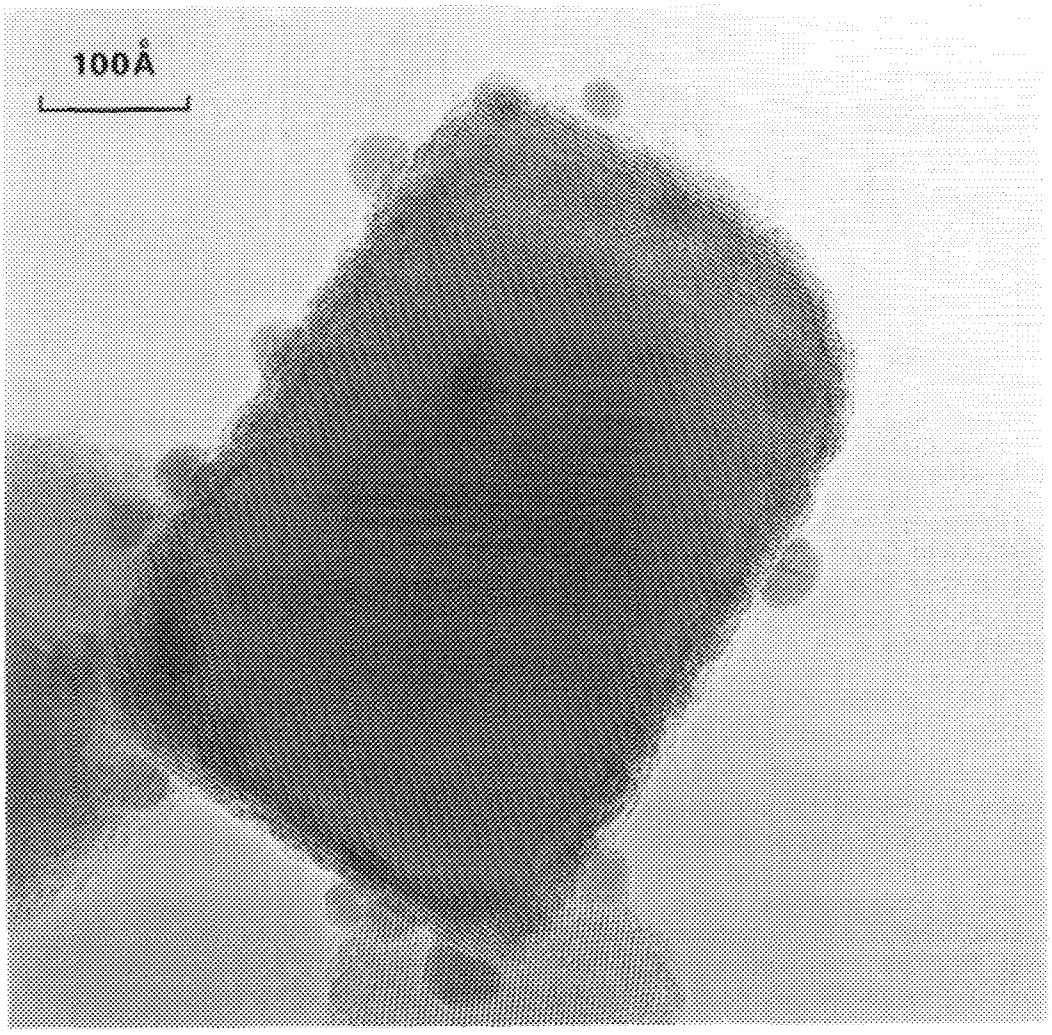

FIG. 5. TEM photograph of Au(3.3 wt%)/TiO_2 prepared by deposition–precipitation followed by calcination at 400°C.

calcined at temperatures below 200°C the conversion of CO at −70°C is very small and it markedly increased at 300°C. We recall the EXAFS data in Fig. 1 which shows that gold is oxidic after calcination at temperatures below 300°C. Taking into account of these observations we may conclude that H_2 oxidation can take place over both oxidic and metallic gold, on the other hand, the presence of metallic gold is indispensable for the low-temperature CO oxidation.

Effect of Support

In Fig. 8 we have plotted the temperatures for 50% conversion of CO (in the abscissa) and H_2 (in the ordinate) in oxidation reactions over a variety of supported gold catalysts and related materials. The central diagonal line corresponds to identical activities for the two reactions. The catalysts above this line are more active for H_2 oxidation and typically are unsupported gold metal, and metals and oxides of Pd and Pt. Sup-

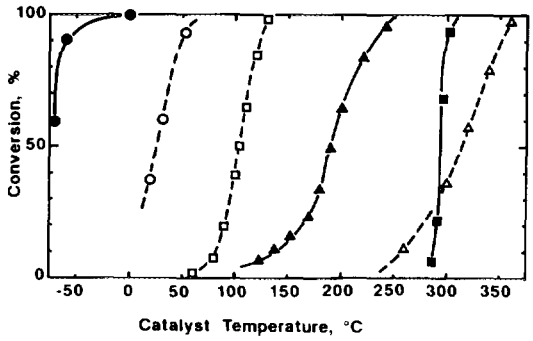

FIG. 6. Conversions of H_2 and CO in catalytic oxidation reactions as a function of catalyst temperature. CO or H_2 1 vol% in air, SV = 2×10^4 h^{-1} · ml/g-cat: oxidation of H_2(○) and CO(●) on Au–Fe(1 : 19) coprecipitate calcined at 400°C in air; oxidation of H_2(□) and CO(■) on Au powder prepared from colloidal metal particles with diameters around 20 nm; oxidation of H_2(△) and CO(▲) on α-Fe_2O_3 powder prepared by calcination of ferric hydroxide at 400°C.

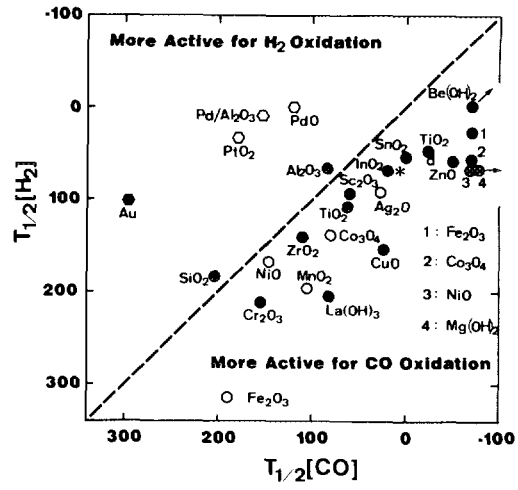

FIG. 8. Temperature for 50% conversion of H_2 and CO in catalytic oxidation reactions over noble metal and metal oxide catalysts: (●) supported gold catalysts calcined at 200–400°C, with metal loadings of 2–5 atom% Au ("d" denotes the samples prepared by deposition–precipitation; the others are prepared by coprecipitation); (*) Au(3.8 wt%)/Al_2O_3 prepared by deposition-precipitation; (○) metal oxides without Au deposition; (○) Pd/Al_2O_3(Pd 0.5 wt%) and oxides of Pt and Pd; (●) gold powder prepared from colloidal metal particles with diameters around 20 nm.

ported gold and simple metal oxides are below this line exhibiting higher activities for CO oxidation, which implys that the catalytic nature of metal oxide supports is reflected in the catalysis of supported gold.

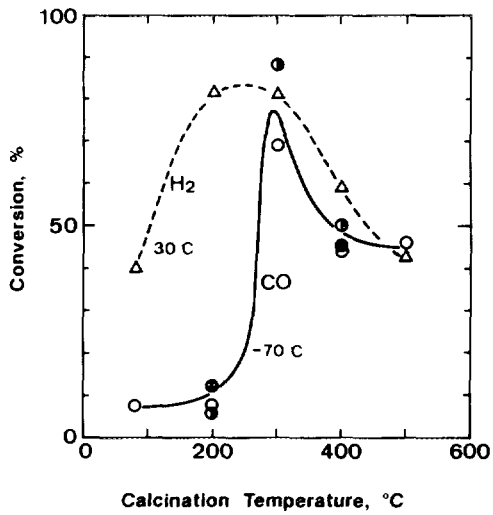

FIG. 7. Conversions of H_2 and CO in catalytic oxidation reactions as a function of calcination temperature of Au–Fe(1 : 19) coprecipitate: (△) H_2 oxidation at 30°C; (○), (◑), (●), CO oxidation at −70°C; the different circles show the data for different precursors prepared in the same manner.

The only exception is gold supported on SiO_2; but SiO_2 is very different from the other supports in the sense that it is a covalently bonded insulator and acidic in nature. It was found that gold could be more highly dispersed on TiO_2 and Al_2O_3 by deposition–precipitation than by coprecipitation and that higher dispersion of gold led to the preferential enhancement in the catalytic activity for CO oxidation. Even in the case of Au/SiO_2, in comparison with unsupported gold the activity is enhanced for CO oxidation although the activity for H_2 oxidation is reduced because of a decrease in gold content.

Among all catalysts able to catalyze CO oxidation at low temperatures, those supported on α-Fe_2O_3, Co_3O_4, NiO, $Be(OH)_2$, and $Mg(OH)_2$ are especially active. It is interesting to note that these are the oxides of Group VIII of 3*d* transition metals and the hydroxides of alkaline earth metals. In

addition, TiO_2 is of peculiar interest since it is poorly active by itself and has been intensively studied in connection with the phenomenon called "strong metal–support interaction" in catalytic systems like Rh/TiO_2 and Pt/TiO_2 (*37–42*) and photocatalysts (*43, 44*). The *n*-type semiconductors such as ZnO and SnO_2 are also of interest for applications to gas sensors (*45*).

Effect of the Particle Size of Gold

Three highly active gold catalysts have been chosen for mechanistic investigations. The reason why we have chosen the three is that the catalytic activities for CO oxidation of the supports differ substantially; TiO_2 is poorly active, Co_3O_4 is the most active, and α-Fe_2O_3 lies between. Figure 9 shows that turnover frequencies (TOFs) based on surface gold atoms are almost independent of the kind of metal oxide support, whereas they are significantly dependent on the particle diameter of gold. The opposite or no appreciable effect of particle size was reported for CO oxidation over Pt, Pd, and Ir supported on SiO_2 and Al_2O_3 (*46–48*), where a decrease in particle size makes the strong adsorption of CO even more intense, with a consequent decrease in TOF. These facts strongly indicate that CO oxidation is structure sensitive on supported gold catalysts but less sensitive or insensitive on Pt-group metal catalysts.

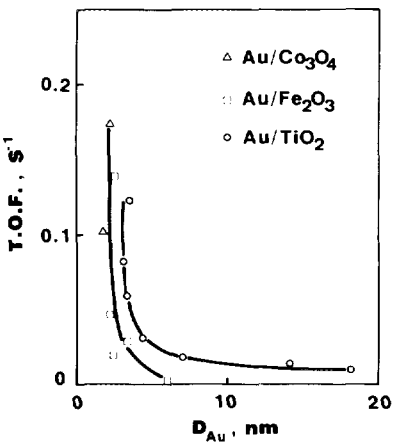

FIG. 9. Turnover frequencies based on surface gold atoms as a function of the mean particle diameters of gold in CO oxidation at 0°C: (△) Au/Co_3O_4, (□) Au/α-Fe_2O_3, and (○) Au/TiO_2.

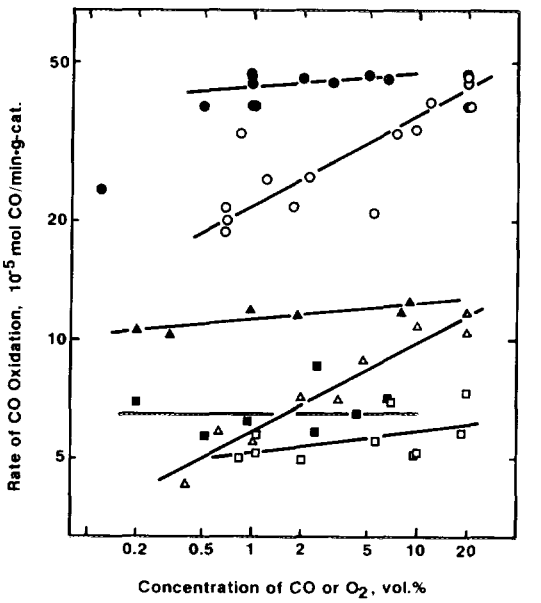

FIG. 10. Rate of CO oxidation as a function of the concentration of CO and O_2: (▲) CO and (△) O_2, Au(1.2 wt%)/Co_3O_4 at 0°C; (■) CO and (□) O_2, Au(0.66 wt%)/α-Fe_2O_3 at 31°C; (●) CO and (○) O_2, Au(3.3 wt%)/TiO_2 at 0°C.

Kinetic Behavior of Supported Gold Catalysts

Figures 10 and 11 show the dependency of the CO oxidation rate on the concentration of CO and O_2, and Arrhenius plots, respectively. The rates of CO oxidation over Au/TiO_2, Au/α-Fe_2O_3, and Au/Co_3O_4 are expressed by the following equations; the apparent activation energies (E_a) are also indicated below:

$$R = k[CO]^{0.05}[O_2]^{0.24},$$

$$E_a = 8.2 \text{ kcal/mol (Au/TiO}_2\text{)}$$

$$R = k[CO]^{0}[O_2]^{0.05},$$

$$E_a = 8.4 \text{ kcal/mol (Au/}\alpha\text{-Fe}_2\text{O}_3\text{)}$$

$$R = k[CO]^{0.05}[O_2]^{0.27},$$

$$E_a = 3.9 \text{ kcal/mol (Au/Co}_3\text{O}_4\text{)}.$$

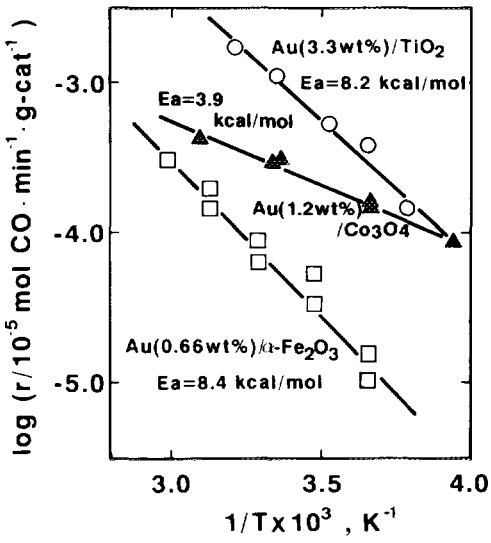

FIG. 11. Arrhenius plots for the rate of CO oxidation over supported gold catalysts: (▲) Au(1.2 wt%)/Co_3O_4, (□) Au(0.66 wt%)/α-Fe_2O_3, and (○) Au(3.3 wt%)/TiO_2.

It is noteworthy to compare these results with the results reported for an unsupported gold sponge in which the rate of CO oxidation corresponded to an order of 0.9 and 0.2 with respect to CO and O_2, respectively, and an activation energy of 3 kcal/mol (*49*). An apparent activation energy of 0 kcal/mol has also been reported for gold wire (*50*). The preexponential factors estimated on the assumption of zero order kinetics were 1.0×10^{25}, 8×10^{23}, 1.9×10^{21} molecules g-cat^{-1} s^{-1} for Au/TiO_2, Au/α-Fe_2O_3, and Au/Co_3O_4, respectively. These values are very large in comparison with the theoretical values, of between 10^{14} to 10^{15} molecules $\cdot$ cm^{-3} s^{-1} for a two molecule reaction, however, they are comparable to the value $2 \times 10^{25+1}$ molecules cm^{-2} Torr^{-1} s^{-1} reported for CO oxidation on Ir(110) under a pressure of $1 \times 10^{-18} - 3 \times 10^{-6}$ Torr and at temperatures below 327°C (*51*).

Temperature-Programmed Desorption of O_2 and CO

Figure 12 shows typical TPD data obtained for Au/TiO_2 and TiO_2. As seen, only a small amount of oxygen is adsorbed over TiO_2 without gold deposition. On the other hand, an appreciable increase is observed in the desorption peak when gold is deposited on TiO_2. The desorption temperature at around 250°C suggests that the surface oxygen species is weakly adsorbed on the surface, most probably as O_2^-. The amount of oxygen desorbed up to 400°C is about 10 μl O_2/g-cat.

For CO TPD studies several doses of CO pulses were injected until excess CO was detected in a He stream and the adsorbed species were then desorbed by raising the temperature. In the case of TiO_2, the amount of CO uptake is small and the desorption takes place as CO at temperatures below 100°C. With the sample containing depos-

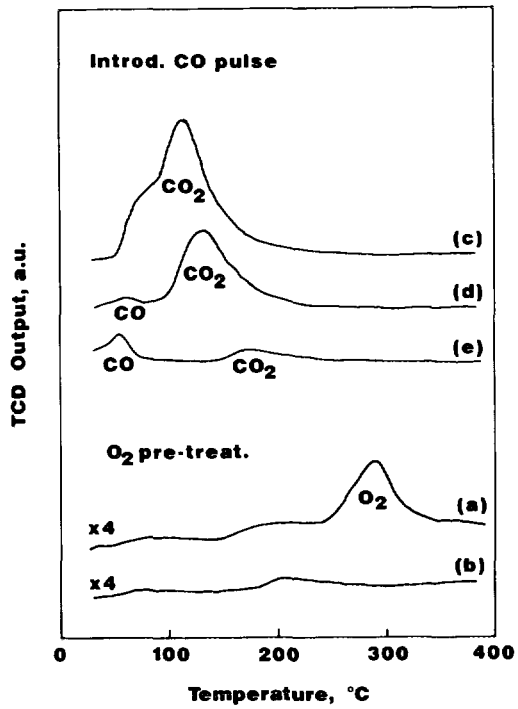

FIG. 12. TPD for Au/TiO_2 (Au loading, 3.3 wt%; D_{Au}, 3.5 nm) and TiO_2. Pretreatment in O_2: (a) Au/TiO_2 and (b) TiO_2. Pretreatment in O_2 or He followed by exposure to CO pulses up to full uptake: (c) Au/TiO_2 in O_2, (d) Au/TiO_2 in He, and (e) TiO_2 in O_2. Heating rate, 10°C/min; rate of flow, 30 ml/min; sample weight, 200 mg.

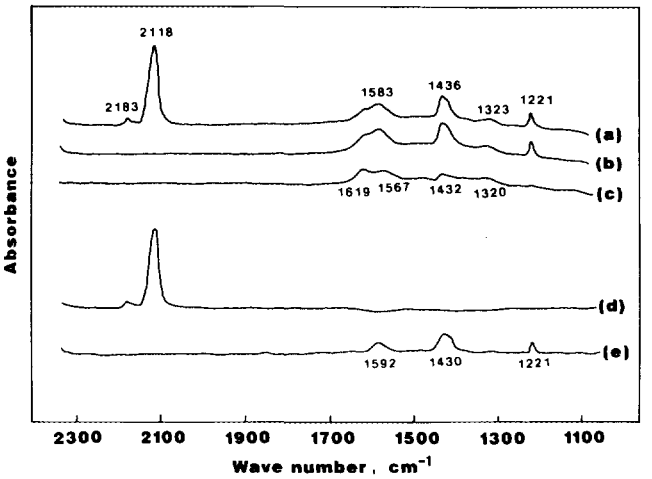

FIG. 13. IR spectra for the adsorbed species of CO on Au/TiO_2 (Au loading, 3.3 wt%; D_{Au}, 3.5 nm) at room temperature. Spectra (a), (b), and (c) were obtained in 30 s, 2 min, and 10 min, respectively, after the injection of a CO pulse into a He stream (5 ml/min). Subtraction spectra: (d) = (a) − (b); (e) = (b) − (c).

ited gold, after O_2 pretreatment, the amount of CO uptake is remarkably increased and desorption always takes place as CO_2 even at low temperatures. When this sample was pretreated in He at 400°C, the amount of CO uptake was appreciably decreased and the desorption at low temperatures evolved CO. This appears to be consistent with the result that vacuum treatment of the catalyst sample appreciably decreased the catalytic activity (*52*). The above results indicate that the uptake of CO can involve oxygen adsorbed on the catalyst surface.

FT-IR Measurements of Surface Adsorbed Species

Figure 13 shows the changes in IR spectra as a function of time for the adsorbed species on Au/TiO_2 when a dose of CO is introduced as a pulse to a He stream at room temperature. Carbon monoxide adsorbed on gold metal and on Ti^{4+} ion are observed at 2118 and 2183 cm^{-1}, respectively. The adsorption of CO appears to be reversible since desorption takes place in 2 min. Carboxylate species observed at 1567 and 1320 cm^{-1} accumulated during the experiment. They might be ascribed to the initial gradual decrease in catalytic activities for fresh samples. Noncoordinated and bidentate carbonate species observed at 1430, 1592 and 1221 cm^{-1}, respectively, disappear in 10 min. The noncoordinated carbonate can be assumed to be formed by the adsorption of reaction product CO_2 from the gas phase. Accordingly, bidentate carbonate is thought to be a reaction intermediate.

DISCUSSION

The present work has clearly demonstrated that thanks to both the small size of the gold particles and the effect of metal oxide supports, supported gold can exhibit extraordinarily high catalytic activity for the low-temperature oxidation of CO. In the following, the reasons for the remarkable properties of this novel catalyst system and the probable mechanism for the genesis of the low-temperature activity will be discussed.

Dominating Factors for Preparing Novel Gold Catalysts

The activities of supported gold catalysts reported by other groups (*9–14*) sometimes differ appreciably from those of ours. As Tanielyan and Augustine have described

(*11*), the activities obtained are indeed very sensitive to the preparation conditions, such as concentration, pH, temperature, aging, and calcination atmosphere. This means that the particle size of the gold, the structure of the gold–metal oxide interface, and the perimeter of the area of contact are noticeably dependent on these conditions. The preparation conditions should be properly selected depending on metal oxide support. For example, active Au/TiO_2 catalysts cannot be obtained by simple coprecipitation (*8*). Magnesium citrate should be added during aging after coprecipitation. It has been found that deposition–precipitation is preferable for the preparation of Au/TiO_2, though the selection of TiO_2 support is also important.

The guidelines for preparing supported gold catalysts with high metal dispersion can be generalized as follows.

1. Gold should be deposited on or mixed with oxide or hydroxide of the support as an hydroxide species which can adhere on the support more strongly than gold metal and chloroauric ions. This requires coprecipitation and deposition–precipitation within the pH range of 6 to 11.

2. Chloride ions should be removed as extensively as possible by repetitive washing of the precursors; the reason is that these ions constitute a strong poison in the catalysis of CO oxidation. The conventional impregnation method is considered to have a serious drawback in this respect as well as in the first point.

3. Final pretreatment or calcination should be carried out in an oxidizing atmosphere (*52*). This is done in order to form metallic gold particles strongly interacting with a metal oxide having an oxygen enriched surface. This feature presents an interesting contrast to the reducing pretreatment used for activating Pt/SnO_2 catalyst (*53*).

Proposed Mechanism

Based on the above experimental results, a mechanism consisting of four steps can be proposed for CO oxidation over supported gold catalysts.

$$CO(g) + S_a \rightarrow CO_{ads}\text{-}S_a, \quad (1)$$

S_a: adsorption sites on Au particles

$$O_2(g) + S_o + e^- \rightarrow O^-_{2ads}\text{-}S_o, \quad (2)$$

S_o: adsorption sites on metal oxide

$$CO_{ads}\text{-}S_a + O^-_{2ads}\text{-}S_o \rightarrow$$

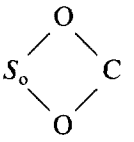

(3)

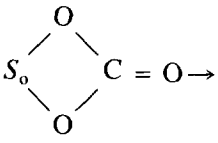

(4)

The zero-order kinetics which we have observed can be interpreted as saturation of adsorbed species (steps (1) and (2)) on a Langmuir surface. The saturation kinetics will give us the following rate expression:

$$R = k[S_a][S_o] \qquad k\text{: constant} \quad (5)$$

$$TOF = R/[S_a] = k[S_o]. \quad (6)$$

Equation (6) indicates that TOFs should be a linear function of the concentration of the sites active for oxygen adsorption. A simple hypothesis is that these sites might be created at the interfacial perimeter around the gold metal particles. If this is the case, $[S_o]$ should increase proportionally to the inverse second power of the particle diameter. This corresponds qualitatively to the results of Fig. 9, where the sharp increase in TOF could correspond to the function of $1/D^2_{Au}$. In the case of Au/TiO_2 and Au/Co_3O_4, the rate of CO oxidation is slightly dependent on the concentration of O_2. This may suggest that over these catalysts the rate of oxygen adsorption does not overwhelmingly predominate over that of carbonate decomposition. The difference compared to $Au/\alpha\text{-}Fe_2O_3$, over which no oxygen pressure dependency is observed, is still unclear; however, it might be ascribed

to enhanced reactivity or adsorption capability of oxygen at the interfacial perimeter.

It seems that there are similarities in the genesis of low-temperature catalytic activities between gold and Pt group metals supported on reducible metal oxides. Schryer *et al.* (*54*) have proposed a well consistent mechanism in which a bicarbonate is formed on a Pt or a Sn site. Although this is not discussed in their paper, it seems probable that the interfacial perimeter constitutes a site for formation of a PtSn alloy during reduction-pretreatment at a relatively low temperature. Riley and his co-workers (*55*) have also proposed that the metal–support interface provides one of the two possible active sites. Sheintuch *et al.* (*56*) have proposed that CO adsorbed on Pd migrates toward the perimeter and there it reacts with oxygen. It is therefore likely that the interfacial perimeter of the noble metal particles play an important role both in SnO_2-supported Pt-group metals and supported gold catalysts. In the context of a previous remark concerning surface mobility, it can be noted that the perimeter might provide new sites for CO adsorption much weaker than on the bare surface of Pt group metals; this would result in an enhanced reaction with oxygen. In the case of supported gold it might provide new sites for O_2 adsorption which hardly takes place on the bare surface of gold. This appears to be consistent with the result that a sputtered gold film on the inside of the discharge tube of CO_2 laser can act as a low-temperature CO oxidation catalyst only in the discharge environment where atomic oxygen or activated oxygen can be created (*57*). Further work should be done on the atomic structure and chemistry of the perimeter to obtain a generalized understanding of the metal–metal oxide interaction and the related catalytic behavior.

CONCLUSION

1. It is not impregnation but coprecipitation and deposition–precipitation that can lead to high dispersion of gold over metal oxide supports.

2. Gold particles, hemispherical in shape, are firmly attached to the support by epitaxial contact, dislocations, or contact with an amorphous layer.

3. Gold–metal oxide combination is indispensable for the genesis of extraordinarily high activities for CO oxidation at temperatures below 0°C.

4. The oxidation of CO over supported gold catalysts is remarkably structure-sensitive.

5. The rate of CO oxidation is independent or only slightly dependent on the partial pressure of CO and O_2.

6. A reaction model is proposed in which CO_2 is produced by the decomposition of bidentate carbonate species, which are formed through the reaction of CO adsorbed on gold, with activated oxygen formed at the interfacial perimeter of the support around the gold particles.

REFERENCES

1. Schwank, J., *Gold Bull.* **16**(4), 103 (1983).
2. Wachs, I. E., *Gold Bull.* **16**(4), 98 (1983).
3. Haruta, M., Yamada, N., Kobayashi, T., and Iijima, S., *J. Catal.* **115**, 301 (1989).
4. Haruta, M., Kageyama, H., Kamijo, N., Kobayashi, T., and Delannay, F., *in* "Successful Design of Catalysts" (T. Inui, Ed.), p. 33. Elsevier, Amsterdam, 1988.
5. Haruta, M., Saika, K., Kobayashi, T., Tsubota, S., and Nakahara, Y., *Chem. Express* **3**(3), 159 (1988).
6. Haruta, M., Kobayashi, T., Iijima, S., and Delannay, F., *in* "Proceedings, 9th International Congress on Catalysis, Calgary, 1988" (M. J. Phillips and M. Ternan, Eds.), p. 1206. Chem. Inst. Canada, Ottawa, 1988.
7. Tsubota, S., Yamada, N., Haruta, M., Kobayashi, T., and Nakahara, Y., *Chem. Express* **5**(6), 349 (1990).
8. Tsubota, S., Haruta, M., Kobayashi, T., Ueda, A., and Nakahara, Y., *in* "Preparation of Catalysts V" (G. Poncelet, P. A. Jacobs, P. Grange, and B. Delmon, Eds.), p. 695. Elsevier, Amsterdam, 1991.
9. Gardner, S. D., Hoflund, G. B., Upchurch, B. T., Schryer, D. R., Kielin, E. J., and Schryer, J., *J. Catal.* **129**, 114 (1991).
10. Takamatsu, S., Ishi-i, M., Imagawa, M., Kinbara, H., Kikuta, T., and Fukushima, T., *Shokubai* (*Catalyst, Cat. Soc. Jpn.*) **34**(2), 126 (1992).

11. Tanielyan, S. K., and Augustine, R. L., *Appl. Catal. A: General* **85,** 73 (1992).
12. Knell, A., Barnickel, P., Baiker, A., and Wokaun, A., *J. Catal.* **137,** 306 (1992).
13. Sze, C., Gulari, E., and Demczyk, B. G., *in* "Nanophase and Nanocomposite Materials," Mater. Res. Soc. Symp. Proc., Vol. 286, p.143. Boston, 1993.
14. Lin, S. D., Bollinger, M., and Vannice, M. A., *Catal. Lett.* **17,** 245 (1993).
15. Haruta, M., *New & Future* **7**(2), 13 (1992). [Published by Jpn. Ind. Technol. Assoc.]
16. Haruta, M., Ueda, A., Tsubota, S., Kobayashi, T., Sakurai, H., and Ando, M., *in* "Proceedings, 1st Jpn.-EC Joint Workshop on the Frontiers of Catal. Sci. Technol., Tokyo, December 1991," p. 173, Organizing Committee JECAT '91.
17. Ueda, A., Kobayashi, T., Tsubota, S., Sakurai, H., Ando, M., Haruta, M., and Nakahara, Y., *in* "Proceedings, 1st Jpn.–EC Joint Workshop on the Frontiers of Catal. Sci. Technol., Tokyo, December 1991," p. 272, Organizing Committee JECAT '91.
18. Ueda, A., and Haruta, M., *Sigen Kankyo Taisaku* (*J. Resources & Environment*) **28**(11), 1035 (1992).
19. Sakurai, H., Tsubota, S., and Haruta, M., *Appl. Catal.*, in press.
20. Frost, J. C., *Nature* **334,** 577 (1988).
21. Lin, S., and Vannice, M. A., *Catal. Lett.* **10,** 47 (1991).
22. Shaw, E. A., Walker, A. P., Rayment, T., and Lambert, R. M., *J. Catal.* **134,** 747 (1992).
23. Baiker, A., Kilo, M., Maciejewski, M., Menzi, S., and Wokaun, A., *in* "Proceedings, 10th International Congress on Catalysis, Budapest, 1992," (L. Guczi, F. Solymosi, and P. Tétényi, Eds.), p. 1257, Elsevier, Amsterdam, 1993.
24. Haruta, M., Takase, T., Kobayashi, T., and Tsubota, S., *in* "Cat. Sci. Techn." (S. Yoshida, N. Takezawa, and T. Ono, Eds.), Vol. 1, p. 331. Kodansha, Tokyo, 1991.
25. Kobayashi, T., Haruta, M., Sano, H., and Nakane, M., *Sensors and Actuators* **13,** 339 (1988).
26. Funazaki, N., Asano, Y., Yamashita, S., Kobayashi, T., and Haruta, M., *Sensors and Actuators B,* **13–14,** 536 (1993).
27. Sato, H. and Tsuchida, E., *Trans. IEICE* **E73** (9), 1525 (1990).
28. Tripathi, A. K., Gupta, N. M., Chatterji, U. K., Iyer, R. M., *Indian J. Technol.* **30**(2), 107 (1992).
29. Zhang, G., Ph.D. thesis, Stanford University, UM8608245, 1985.
30. Buffat, Ph., and Borel, J-P., *Phys. Rev. A.* **13**(6), 2287 (1976).
31. Maeda, H., Terauchi, H., Tanabe, K., Kamijo, N., Hida, M., and Kawamura, H., *Jpn. J. Appl. Phys.* **21,** 1342 (1982).
32. Berlowitz, P. J., Peden, C. H. F., and Goodman, D. W., *J. Phys. Chem.* **92,** 5213 (1988).
33. Wagner, F. E., Tsubota, S., and Haruta, M., unpublished data.
34. Miyamoto, A., Haruta, M., and Inui, T., *in* "Cat. Sci. Techn." (S. Yoshida, N. Takezawa, and T. Ono, Eds.), Vol. 1, p. 497. Kodansha, Tokyo, 1991.
35. Tanaka, N., Mihama, K., Tsubota, S., and Haruta, M., *in* "Proc. 46th Annual Meet. of Phys. Soc. of Japan, Hokkaido Univ., 1991," 30aL-13.
36. Wagner, C. D., Riggs, W. M., Davis, L. E., Moulder, J. F., and Muilenberg, G. E., "Handbook of X-ray Photoelectron Spectroscopy," Perkin–Elmer Co., Eden Prairie, 1979.
37. Baker, R. T. K., Tauster, S. J., and Dumesic, J. A., "Strong Metal–Support Interactions," ACS Symposium Series, Vol. 298, Amer. Chem. Soc., Washington, DC, 1986.
38. Schwank, J., Shastri, A. G., and Lee, J. Y., *in* "Strong Metal–Support Interactions," ACS Symposium Series, Vol. 298, p. 182. Amer. Chem. Soc., Washington, DC, 1986.
39. Tauster, S. J., *Acc. Chem. Res.* **20,** 389 (1987).
40. Stevenson, S. A., "Metal–Support Interactions in Catalysis, Sintering, and Redispersion." Van Nostrand–Reinhold, New York, 1987.
41. Haller, G. L., and Resasco, D. E., *in* "Advances in Catalysis," (D. D. Eley, H. Pines, and P. B. Weisz, Eds.), Vol. 36, p. 173. Academic Press, San Diego, 1989.
42. Williams, K. J., Boffa, A. B., Levin, M. E., Salmeron, M., Bell, A. T., and Somorjai, G. A., *Catal. Lett.* **5,** 385 (1990).
43. Gao, Y-M., Treham, R., Kershow, R. Dwight, K., and Wold, A., *Mater. Res. Bull.* **26,** 1247 (1991).
44. Kanno, H., Yamamoto, Y., and Harada, H., *Chem. Phys. Lett.* **121**(3), 245 (1985).
45. Kobayashi, T., Haruta, M., and Sano, H., *Chem. Express* **4**(4), 217 (1989).
46. Che, M., and Bennet, C. O., *in* "Advances in Catalysis," (D. D. Eley, H. Pines, and P. B. Weisz, Eds.), Vol. 36, p. 55. Academic Press, San Diego, 1989.
47. Ichikawa, S., Poppa, H., and Boudart, M., *in* "Catalytic Materials: Relationship Between Structure and Reactivity" (T. E. Whyte, Jr., R. A. Dalla Betta, E. G. Derouane, and R. T. K. Baker, Eds.), ACS Symp. Series, Vol. 248, p. 439. Amer. Chem. Soc., Washington, DC, 1984.
48. Oh, Se H. and Eickel, C. C., *J. Catal.* **128,** 526 (1991).
49. Cant, N. W., and Fredrickson, P. W., *J. Catal.* **37,** 531 (1975).
50. Daglish, A. G., and Eley, D. D., *in* "Proceedings, 2nd International Congress on Catalysis, Paris, 1960," p. 1615. Techip, Paris, 1961.
51. Taylor, J. L., Ibbotson, D. E., and Weinberg, W. H., *J. Catal.* **62,** 1 (1980).
52. Cunningham, D., Tsubota, S., Kamijo, N., and Haruta, M., *Res. Chem. Interm.* **19**(1), 1 (1993).
53. Schryer, D. R., Upchurch, B. T., Van Norman,

J. D., Brown, K. G., and Schryer, J., *J. Catal.* **122,** 193 (1990).

54. Schryer, D. R., Upchurch, B. T., Sidney, B. D., Hoflund, G. B., and Herz, R. K., *J. Catal.* **130,** 314 (1991).
55. Dawood, T., Richmond, J. R., and Riley, B. W., "Low-Temperature CO-Oxidation Catalysts for Long-Life CO_2 Lasers," NASA Conference Publication 3076, p. 157, 1990.
56. Sheintuch, M., Schmidt, J., Lecthman, Y., and Yahav, G., *Appl. Catal.* **49,** 55 (1989).
57. Macken, J. A., Yagnic, S. K., and Samis, M. A., *IEEE J. Quantum Electron.* **25**(7), 1695 (1989).